Scaling laws of compliant elements for high energy storage capacity in robotics

Saerens, Elias; Furnémont, Raphaël Guy; Verstraten, Tom; Lopez Garcia, Pablo; Crispel, Stein; Ducastel, Vincent; Vanderborght, Bram; Lefeber, Dirk

Published in:
Mechanism and Machine Theory

DOI:
10.1016/j.mechmachtheory.2019.05.013

Publication date:
2019

License:
Unspecified

Document Version:
Submitted manuscript

Scaling laws of compliant elements for high energy storage capacity in robotics

Article *in* Mechanism and Machine Theory · September 2019

DOI: 10.1016/j.mechmachtheory.2019.05.013

8 authors, including:

Elias Saerens
Vrije Universiteit Brussel
13 PUBLICATIONS **10** CITATIONS
SEE PROFILE

Raphaël Furnémont
Vrije Universiteit Brussel
27 PUBLICATIONS **298** CITATIONS
SEE PROFILE

Tom Verstraten
Vrije Universiteit Brussel
50 PUBLICATIONS **310** CITATIONS
SEE PROFILE

Pablo Lopez Garcia
Vrije Universiteit Brussel
15 PUBLICATIONS **35** CITATIONS
SEE PROFILE

Scaling laws of compliant elements for high energy storage capacity in robotics

Elias Saerens[1,*], Raphaël Furnémont[1], Tom Verstraten[1], Pablo López García[1], Stein Crispel[1], Vincent Ducastel[1], Bram Vanderborght[1] and Dirk Lefeber[1]

***Abstract*—The key component in compliant actuators is the elastic element, typically a spring. Nevertheless, different types of springs have different characteristics in terms of size, weight, maximum allowable force, maximum allowable torque and maximum allowable deflection. It is however very important to compare them on these requirements, since each application has other demands. In this paper, the energy storage capacity of different types of compliant elements are calculated using scaling laws in order to easily derive the maximum achievable energy capacity for a certain arrangement. These scaling laws are given as a function of the structural parameters and are validated with catalog data of spring manufacturers and distributors such as Alcomex, Lesjöfors and Century Spring. As such, different types of compliant elements can be compared in an easy way. To fully exploit the capabilities of compliant elements, these scaling laws are used to verify the effect of spring parallelization on mass and/or enclosed volume, which is interesting regarding redundant compliant actuation. From theoretical calculations and a case study, it follows that parallelization is beneficial, especially for mass reduction.**

Keywords*—*Scaling laws, compliant actuation, parallel arrangements, energy storage capacity

I. INTRODUCTION

The incorporation of compliant elements into actuators has led to the development of compliant actuators [1]. They demonstrate improved shock-resistance, torque-to-mass ratio, power-to-mass ratio and energy efficiency in comparison with stiff actuators. These last two properties are particularly important in novel robotic applications, like exoskeletons, prostheses or co-bots, which require actuators with high efficiency, torque-to-mass ratio, power-to-mass ratio and a safe Human-Robot-Interaction (HRI) [2].

Different types of springs are used in compliant actuators in order to grant these characteristics. Some actuators use springs that can easily be found in catalogs, like compression springs [3], [4], tension springs [5] and torsion springs [6], [7]. However, some actuators need custom-made springs, like spiral springs [8] and torsion springs [9–11] to respond more adequately to the needs of their design. Leaf springs are also a type of springs that need to be custom-made [12–15]. This is due to the fact that there is so much variety that no standard models are offered in catalogs of manufacturers. In some cases also more exotic springs are used in the design of actuators. Examples of this are e.g. disc springs [16], torsion rods [17] and elastic bands [18].

Considering all these compliant elements, several studies address the optimal selection of compliant elements. These studies are generally based on constrained optimization, where the spring is designed in order to minimize the mass, using usually either genetic algorithms [19–21] or particle swarm optimization [22]. For these methods only design parameters were used. In [23] also dynamic parameters (e.g. natural frequencies, dynamic response) were added to this optimization process. In [24–27] the springs were also designed to match the natural motion, but here to minimize the power consumption instead of the mass.

These studies are however exclusively made for helical (compression) springs and consider only one spring in their design. Nevertheless, it is also possible to use several springs in parallel, e.g. one big spring can be replaced by several smaller ones in parallel that in total give the same output characteristics. This principle of parallelization is used in the Series Parallel Elastic Actuator (*SPEA*) [28]. This type of actuator shows even better properties in terms of energy efficiency [29] than standard compliant actuators, like e.g. SEAs [1]. In these redundant actuators different types of springs can be used. The first prototypes of the SPEA used tension springs, but the latest developments include spiral springs [30].

Investigating the properties of redundant systems is interesting, but to see if these actuators are better in general, a tool is needed to verify the influence of parallelization and whether this is positive or not in terms of mass and/or volume reduction.
In this paper, these problems will be tackled by the use of scaling laws. This will be done by studying how the energy storage capacity of compression and torsion springs (both helical and spiral) scales with their principal dimensions and mass. The energy storage capacity will be used as metric of comparison, since it includes the influence of both torque, force and elongation/deflection, which is needed for a fair comparison. It also is shown in other works that this is an important metric for compliant actuators [31], [32].

The structure of the paper is as follows. First, in section II the scaling of the energy storage capacity for helical springs, i.e. compression and helical torsion springs, will be derived based on their design equations. All these scaling models will be validated with catalog data. Afterwards, in

[1] Robotics & Multibody Mechanics Research Group (R&MM), Department of Mechanical Engineering, Vrije Universiteit Brussel (VUB) and Flanders Make, 1050 Brussels, Belgium.
*Corresponding Author: elias.saerens@vub.be (Elias Saerens)
Preprint submitted to Mechanism and Machine Theory

section III, the derivation of the same characteristics will be elaborated for flat springs. The laws derived in this section will also be compared to existing catalog data. To address the effectiveness of redundant systems, the theoretical influence of parallelization for all mentioned springs will be investigated in section IV in order to see if it is beneficial in terms of volume and mass requirements. This influence will be more elaborated in section V, where the practical design of a compression spring arrangement will be tackled.

To conclude this analysis, a general discussion will be given in section VI. This discussion will start by explaining why some types of springs are not discussed in this paper and goes further by comparing all treated springs. This section will be closed by providing an overview table which provides some guidelines for spring design/selection when the energy storage capacity needs to be optimized. Then to finish, in section VII, a conclusion will be given about what can be concluded from the results and which will be the future work.

II. SCALING FOR HELICAL SPRINGS

A. Introduction

In this section the scaling of helical compliant elements will be investigated based on the stress equations of springs. The needed equations are based on the ones found in [33–35]. The parameters involved in these equations are summarized in Table I. When the scaling laws are derived, they will be validated, using spring catalog data from Alcomex, Lesjöfors and Century Spring.

Symbol	Explanation	Unit
τ_{max}	Maximum shear stress	Pa
σ_{max}	Maximum normal stress	Pa
$\tau_{c,zul}$	Maximum allowed shear stress	Pa
R_m	Maximum tensile strength	Pa
$\sigma_{c,zul}$	Maximum allowed normal stress	Pa
P	Load applied on the spring	N
φ	Angular deflection of the spring	rad
M	Torque applied on the spring	Nm
D	Mean diameter of the spring	m
d	Wire diameter	m
K	Shear stress correction factor	/
C	Spring index ($=\frac{D}{d}$)	/
A, B	Empirical coefficients	/
δ	Elongation of the spring	m
G	Module of rigidity	N/m^2
E	Module of elasticity	N/m^2
V	Enclosed volume of the spring	m^3
n	Number of active coils	/
U	Energy stored in the spring	J
n_t	Total number of coils	/
ρ	Density of the spring material	kg/m^3
m	Mass of the spring	kg
L_0	Length of the spring at no-load	m
N	Number of springs	/

TABLE I: Nomenclature of helical springs

B. Compression springs

A compression spring together with its symbols used to describe them can be seen in Fig. 1. The specific equations used in this for this type of springs are shown in Table. II.

There are additional equations that are used to check whether the springs can buckle, but since most of the time the theoretical approach will be combined with springs from catalogs, these equations will not be taken into account. Depending on the application it can also be required to check if surge will appear. To prevent this, the resonance frequency of the spring itself should be large enough with respect to that of the load. The surge phenomenon is however not relevant, since it only happens at high frequencies, which is not the working range of compliant actuators.

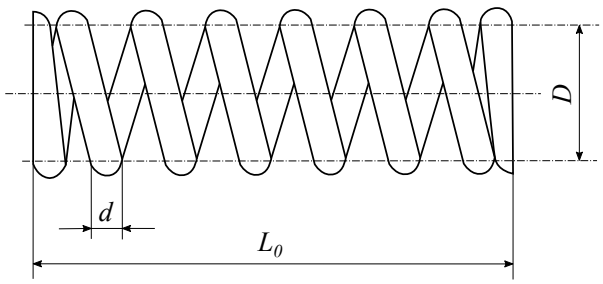

Fig. 1: Representation of compression springs and the symbols used to describe them.

$$\tau_{max} = K\frac{8PD}{\pi d^3} \quad (1)$$

$$\tau_{c,zul} = 0.56R_m \quad (2)$$

$$U = \frac{1}{2}P\delta \quad (3)$$

$$m \approx \rho(\pi Dn)(\pi\frac{d^2}{4}) \quad (4)$$

$$L_0 = nd + \delta \quad (5)$$

$$K = K_W = \frac{4C-1}{4C-4} + \frac{0.615}{C} \quad (6)$$

$$R_m = A_m - B_m \log d \quad (7)$$

$$\delta = \frac{8PC^3n}{Gd}\left(1+\frac{0.5}{C^2}\right) \quad (8)$$

$$V \approx \frac{L_0\pi(D+d)^2}{4} \quad (9)$$

TABLE II: Equations of helical compression springs.

Some remarks can be made regarding the equations presented in Table II:

- The volume of the spring wire (needed to calculate the mass) is approximated by the volume of n tori of diameter d where the mean diameter of the spring D becomes the distance from the center of the torus to the center of the tube.
- The number of active and total coils will be assumed to be the same, hence $n = n_t$. In practice, the difference between the number of active and total coils is comprised between one and two, depending on the type of ending of the springs (e.g. grounded, grounded and closed for compression springs, etc...).
- K is the Wahl's stress correction factor ($K_W = \frac{4C-1}{4C-4} + \frac{0.615}{C}$). Another correction factor, defined by Bergsträsser ($K_B = \frac{C+0.5}{C-0.75}$), can also be used.
- The term $\left(1+\frac{0.5}{C^2}\right)$ in (8) is generally close to 1 and will thus be neglected. In standards, it is not even accounted.

Now, for compression springs the shear stress on the coils needs to be lower or equal to the maximum allowable shear stress of the material, since otherwise they will be damaged and break. Hence:

$$\tau_{max} \leq \tau_{c,zul} = 0.56 R_m \tag{10}$$

The maximum allowable shear stress is given by (2) and (7). This is almost half of the maximum tensile strength in order to incorporate the effect of fatigue. Eq. (7) is an empirical law, where the coefficients A_m and B_m depend on the material. These coefficients can be found in standards such as EN 1270-1. The logarithmic law provided is difficult to handle and thus the first step of this work, in order to ease the theoretical approach, is to replace the logarithm in (7) by a power law, such that (2) becomes:

$$\tau_{c,zul} = A d^B \tag{11}$$

A comparison is made between a logarithmic and power law in Fig. 2.

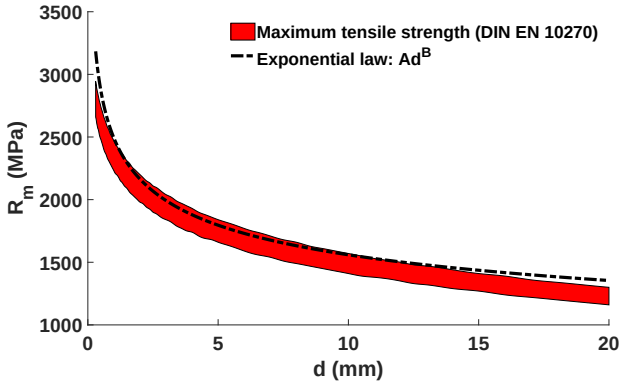

Fig. 2: The red area gives the limit of the maximum tensile strength for cold drawn unalloyed spring steel wire according to the norm EN 1270-1. An exponential law (dark dashed line) provides a good approximation of the upper/lower bound of the tensile strength. Note that the coefficients of the exponential law (A, B) can be adapted depending on the range of d in order to have a better approximation.

The coefficients of the power and logarithmic laws (the coefficients B) are negative, indicating that the maximum shear stress that can be applied on a coil increases as the coil diameter d decreases. The limit, given by (7) from standards (as DIN EN 10270), serves as a guideline for manufacturers. Generally, the maximum tensile stress for springs following this standard is lower, but follows a logarithmic/exponential trend. This means that the development proposed here is coherent. A table of the different coefficients A and B for compression springs of different catalogs is given in Table III.

Catalog		Power law: Ad^B		R^2
		$A/1e6$	B	
Alcomex [36]		229.1	-0.2528	0.998
Lesjöfors [37]	EN 10270-1-SM	132.6	-0.2137	0.985
	EN 10270-3-4310	144.5	-0.1888	0.972
	Swedish standard	155	-0.2291	0.949
	DIN 2098	207.7	-0.242	0.998
Century Spring [38]	Music Wire	145.5	-0.2733	0.958
	Spring Steel	89.85	-0.3071	0.936
	Hard Drawn	1.161	-0.2529	0.85
	Stainless Steel	71.45	-0.3248	0.961

TABLE III: Coefficients A and B for different compression springs proposed in catalogs.

1) Energy storage capacity vs. Mass:

In this section, it will be assumed that the springs are designed in such a way that they can withstand the highest shear stress possible. Hence, $\tau_{max} = \tau_{c,zul}$. Following this assumption, first an expression for the load on the spring (P) needs to be found using Eq. (1).

$$\tau_{max} = K \frac{8PD}{\pi d^3} = A d^B \rightarrow P = \frac{\pi A d^{3+B}}{8KD} \tag{12}$$

Knowing that the energy stored in a spring (U) is calculated by $U = \frac{1}{2} P \delta$ and combining it with (8) and (12) (neglecting the term in brackets as mentioned before), the stored energy for compression springs can be expressed as follows:

$$U = \frac{1}{4} \frac{A^2 d^{2B}}{\rho K^2 G} m \tag{13}$$

By using Eq. (4), the wire diameter can be written as a function of the mass:

$$d = \sqrt[3]{\frac{4m}{\rho \pi^2 C n}} \tag{14}$$

By inserting Eq. (14) into (13) one gets:

$$U = \frac{1}{4} \frac{A^2}{\rho G K^2} \left(\frac{4}{\rho \pi^2} \right)^{\frac{2B}{3}} (Cn)^{\frac{-2B}{3}} m^{\frac{2B+3}{3}} \tag{15}$$

If we now want to see the maximum energy density as a function of the mass, the limitations of some parameters in Eq. (13) need to be checked.

Regarding the spring index C, it can be noted that it is limited in practice to $C \in [4;22]$. This is also reflected in different standards, e.g. $C \in [3;12]$ for ISO 11891:2012. Also, a small spring index can result in excessive local stresses, while a high spring index leads to springs that are flimsy and tangle more easily. As a result, the shear stress correction factor (K) is also bounded:

$$K \in [1,06;1,40] \rightarrow K^{-2} \in [0,51;0,88]$$

To achieve a maximal energy capacity, it can be seen in Eq. (15) that K should be minimal.

Due to limitations in the manufacturing process the number of coils n is also limited.

Following the aforementioned remarks, it is clear that the term $K^{-2}(Cn)^{\frac{-2B}{3}}$ is bounded, meaning that the maximum energy capacity as a function of the mass will be found by taking the maximum of $K^{-2}(Cn)^{\frac{-2B}{3}}$. This is achieved by taking the maximum number of coils (n) and the maximum spring index (C). This has also an extra influence due to the K-factor, since that needs to be minimized, which is exactly what happens when maximizing C.

From Eq. (13), it can be concluded that the maximum gravimetric energy density is achieved by having a minimal wire diameter d (since B in the exponent is always negative). Hence, for a certain mass m, the maximum possible energy capacity can be achieved using a minimal wire diameter d, which is given by:

$$d_{min} = \sqrt[3]{\frac{4m}{\rho\pi^2 C_{max} n_{max}}} \tag{16}$$

As the mass increases, the minimum value of d also increases. Knowing all this, Eq. (15) can be used to see how the energy capacity evolves as a function of the mass. This behaviour is depicted in Fig. 3.

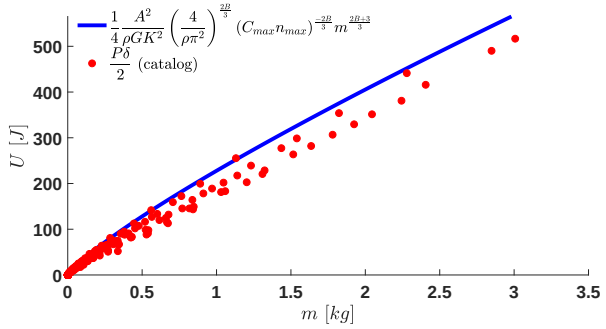

Fig. 3: The red dots represent the energy storage capacity of compression springs as a function of their mass. This data is extracted from the catalog data of Alcomex [36]. The blue line represents the maximum energy capacity as a function of the mass according to Eq. (15). The maximum number of coils and maximum spring index in the catalog were taken for C and n.

This shows the potential of a configuration using springs placed in parallel. A spring with a given mass can be replaced by a combination of several springs, for the same extension and stiffness (thus the same energy stored), but with a total mass that is reduced. How the springs are integrated into the mechatronic design largely depends on the system, but we propose corrective factors, based on development presented in section V, to give a rough idea on how it influences the total mass.

*2) **Energy storage capacity vs. Volume**:*

In this subsection, the energy storage capacity will be compared with the volume. This volume represents the enclosed volume, i.e. the total volume the spring takes when in uncompressed condition and hence not just the volume of the wire.

To write the energy capacity as a function of the enclosed volume, first the full expression of the volume should be derived. By combining Eqs. (5), (9) and (12), it can be found that the volume is given by:

$$V = \frac{\left[KG + \pi A d^B C^2\right](1+C)^2 d^3 \pi n}{4KG} \tag{17}$$

By doing some small calculations, similarly to what was done for the energy calculation in function of the mass, it can be found that, using Eq. (17), the energy capacity as a function of the enclosed volume is given by:

$$U = \left(\frac{\pi A^2 d^{2B} C}{4K(1+C)^2\left[KG + \pi A d^B C^2\right]}\right) V \tag{18}$$

Now normally the wire diameter in this equation should be replaced, using Eq. (17), so it can be written as a function of the enclosed volume. It can however be seen that it is not possible to do this, since 'd' can not be filtered out in Eq. (17). To cope with this problem, an approximation will be made.

It can be found that (KG) and $(\pi A d^B C^2)$ have a similar magnitude, but with a small factor between them. For the small wire diameters they can be considered equal (i.e. a factor $w = 1$). For the biggest wire diameters this ratio becomes approximately 9. Due to this, (KG) can be replaced by the other term and the wire diameter can be written as a function of the volume as follows:

$$d = \sqrt[3+B]{\frac{4KGV}{(w+1)\pi^2 A C^2 (1+C)^2 n}} \tag{19}$$

By inserting Eq. (19) into (18) (replacing again (KG)) one gets:

$$U = \left(\frac{A}{4K}\right)^{\frac{3}{3+B}}\left(\frac{G}{n\pi^2}\right)^{\frac{B}{3+B}}(C)^{\frac{-3-3B}{3+B}}\left((w+1)(1+C)^2\right)^{\frac{-3-2B}{3+B}} V^{\frac{3+2B}{3+B}} \tag{20}$$

Now, regarding Eq. (20), it can be seen that in order to maximize the energy capacity as a function of the volume, two different things have to be done. The spring index should be minimized and, since the coefficient B is always negative, the number of coils should be maximized.

When looking at Eq. (18) it can be seen that the same claims hold true together with the fact that the wire diameter should be minimized. However, when looking to Eq. (19) it can be noted that, in order to minimize the wire diameter, the spring index should now be maximized. Having to take the spring index (C) maximal is in contrast with what is derived from (18), but due to the interdependency between d, n and C, no uniform decision can be taken about which C is needed to achieve the maximal energy capacity.

Hence, due to practicalities, a trade off between d and C should be made in the design of the spring, based on the shape and available space.

It can be seen that this holds true in Fig. 4, since for low volumes (where small wire diameters are used) the maximal energy capacity can indeed be predicted using the factor $w = 1$ in Eq. (20). On the other hand, the maximal energy capacity for the biggest volume in the catalog (which needs a bigger wire diameter) can, on the other hand, be predicted using the maximal factor $w = 9$.

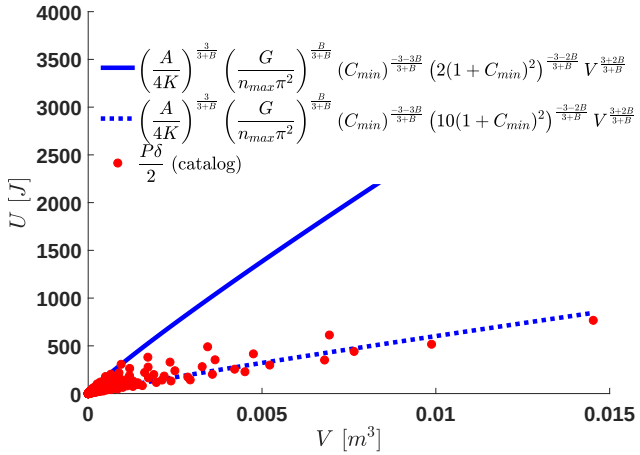

Fig. 4: The red dots represent the energy storage capacity of compression springs as a function of their enclosed volume. This data is extracted from the catalog data of Alcomex [36]. The full blue line represents the maximum energy capacity according to (20), when using a minimal spring index C, a maximal number of coils n and a factor $w = 1$. The dotted blue line is the same, but now uses a factor $w = 9$. It can be observed that, as expected, the maximum energy capacity for low volumes is best approximated with the line made using $w = 1$ and for high volumes w has to increase till a maximum of 9.

C. Torsion springs

Together with compression and tension springs, torsion springs also fit in the helical spring category due to their intrinsic shape. The difference with the previous two is the way the load is applied. For torsion springs, the load is applied on the end of the wire, which goes outside the helical shape like a leg. Due to this, the spring may be subject to torque around the coil axis. As a consequence,the primary stress is flexural while, in contrast with compression springs, the primary stress is torsional.

A torsion spring together with the nomenclature used to describe it can be seen in Fig. 5. The equations used in this section are shown in Table. IV.

Due to helical shape, the derivations for torsion springs will be similar and the same assumptions can be taken as in section II-B.

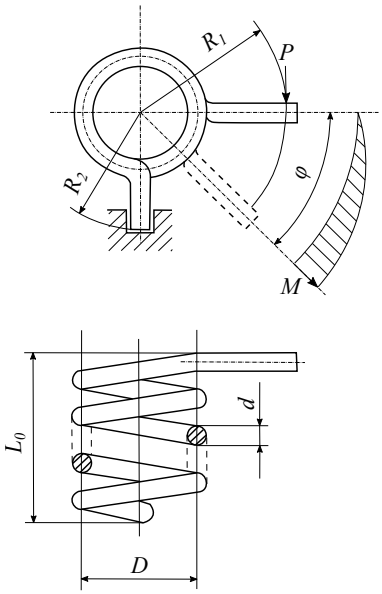

Fig. 5: Representation of torsion springs and the used nomenclature.

$$\sigma_{max} = K\frac{32M}{\pi d^3} \quad (21)$$

$$\sigma_{zul} = 0.70R_m \quad (22)$$

$$U = \frac{1}{2}M\varphi \quad (23)$$

$$m \approx \rho(\pi Dn)(\pi\frac{d^2}{4}) \quad (24)$$

$$K = K_T = \frac{4C^2 - C - 1}{4C(C-1)} \quad (25)$$

$$R_m = A_m - B_m \log d \quad (26)$$

$$\varphi = \frac{64MDn}{Ed^4} \quad (27)$$

$$V \approx \frac{\pi nd(D+d)^2}{4} \quad (28)$$

TABLE IV: Equations of helical torsion springs

Again, in order to ease the theoretical approach, the logarithm in (26) is replaced by a power law, such that (22) becomes:

$$\sigma_{zul} = Ad^B \quad (29)$$

A table of the different coefficients A and B for springs of different catalogs is given in Table V.

Catalog		Power law: Ad^B		R^2
		$A/1e6$	B	
Alcomex [36]		550.4	-0.121	0.976
Century Spring [38]	Music Wire	439.1	-0.1681	0.895
	Stainless Steel	1265	-0.165	0.888

TABLE V: Coefficients A and B for different torsion springs proposed in catalogs.

1) *Energy storage capacity vs. Mass:*

To start, again an expression should be found to describe the load in function of the wire diameter. This can be done knowing that, for helical torsion springs, the assumption can

also be made that its maximum tensile strength can be written as a power law. Hence, by combining Eqs. (21), (22) and (26), the following relation can be found:

$$\sigma_{max} = K\frac{32M}{\pi d^3} = Ad^B \rightarrow M = \frac{\pi A d^{3+B}}{32K} \tag{30}$$

Knowing that $U = \frac{1}{2}M\varphi$, combined with Eqs. (30) and (27), it can be derived that the energy capacity inside a torsion spring is given by:

$$U = \frac{A^2 d^{2B}}{8\rho K^2 E} m \tag{31}$$

By inserting Eq. (24) into (31), one gets:

$$U = \frac{A^2}{8\rho K^2 E} \cdot \left(\frac{4}{\rho n C \pi^2}\right)^{\frac{2B}{3}} m^{\frac{2B+3}{3}} \tag{32}$$

Following the same procedure as for compression springs, it is clear that the term $(Cn)^{\frac{-2B}{3}}$ is bounded, meaning that the maximum gravimetric energy density as a function of the mass will be found by taking the maximum of $(Cn)^{\frac{-2B}{3}}$. So both the number of coils and the maximum spring index should be maximized.

Remembering that the spring index C is limited in practice to $C \in [4;22]$, it can be seen that K is again bounded:

$$K \in [1.04;1.23] \rightarrow K^{-2} \in [0.66;0.93]$$

Knowing all this, Eq. (32) can be used to see how the energy capacity evolves as a function of the mass. This behaviour is depicted in Fig. 6.

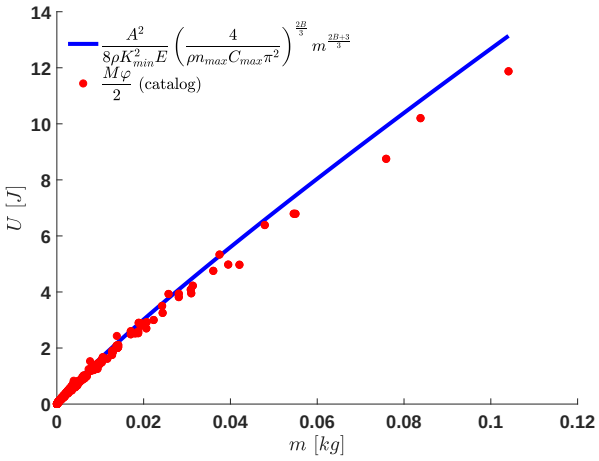

Fig. 6: The red dots represent the energy storage capacity of torsion springs as a function of their mass. This data is extracted from catalog data (Century Spring - Music Wire) [38]. The blue line represents the maximum energy storage capacity according to Eq. (32). The maximum number of coils and maximum spring index in the catalog were taken for C and n. For the stress correction coefficient K, the minimum is taken.

*2) **Energy storage capacity vs. Volume**:*

After some small calculations it can be found that the energy capacity, as a function of the volume, is given by:

$$U = \frac{\pi A^2 C}{8K^2 E}\left(\frac{4}{n\pi}\right)^{\frac{2B}{3}} (1+C)^{\frac{-4B-6}{3}} V^{\frac{2B+3}{3}} \tag{33}$$

It can be seen that in order to find the maximum energy storage capacity as a function of the volume, the number of coils again needs to be maximized. However, the choice of the spring index is less obvious due to the fact that C appears in several factors (i.e. C, $(1+C)^{\frac{-4B-6}{3}}$ and $1/K^2$). When plotting the product of these factors, it can be seen clearly that (considering the practical limit) C should always be minimized in order to reach a maximal energy storage capacity This behaviour is depicted in Fig. 7.

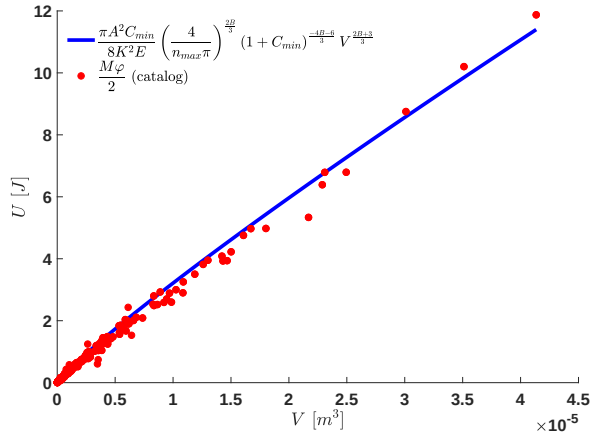

Fig. 7: The red dots represent the energy storage capacity of torsion springs as a function of their enclosed volume. This data is taken from a catalog (Century Spring - Music Wire) [38]. The blue line represents the maximum energy storage capacity according to Eq. (33). The maximum number of coils and minimum spring index in the catalog were taken for n and C.

III. SCALING FOR FLAT SPRINGS

A. Introduction

Flat spring is the generic term given to springs that are made of a flat strip of metal, i.e. material with a high width-to-thickness ratio. Unlike helical springs, flat springs can be used to combine several functions, since different shapes can easily be made. Due to this variety, the number of flat springs that will be discussed in this section will be limited to the most general ones from which catalog values exist, i.e. spiral springs and constant force springs.

In this section, the scaling of flat compliant elements will be investigated based on the stress equations of springs. The equations used here are based on the ones found in [33] and [34]. The parameters that are used in the calculations of flat springs are summarized in Table VI. At the end of each subsection, the scaling laws will be compared to spring catalog data from Lesjöfors.

Symbol	Explanation	Unit
σ_{max}	Maximum normal stress	Pa
$\sigma_{c,zul}$	Maximum allowed normal stress	Pa
R_m	Maximum tensile strength	Pa
b	Width of the spring strip	m
t	Thickness of the spring strip	m
L	Length of the spring strip	m
φ	Angular deflection of the spring	rad
M	Torque applied on the spring	Nm
P	Load applied on the spring	N
E	Module of elasticity	N/m^2
a	Inter-coil distance	m
R_i	Inner radius of the spring	m
R_o	Outer radius of the spring	m
V	Enclosed volume of the spring	m^3
U	Energy stored in the spring	J
m	Mass of the spring	kg
N	Number of springs	/
n	Number of active coils	/
n_t	Total number of coils	/
ρ	Density of the spring	kg/m^3
K_b	Curvature correction factor	/
A, B, α, γ	Empirical coefficients	Pa

TABLE VI: Nomenclature of flat springs

B. Spiral torsion springs

A spiral torsion spring (also sometimes called 'Hair spring' or 'Clock spring') is a flat strip of metal that is wound up in a spiral shape. For this type of springs, the loads are applied to the inner and outer end of the spiral, and the produced torque is determined by the angular change between both extremities. Due to the fact that the load is applied on the entire width of the flat strip, which is normally a lot higher than the thickness, the connection contact stresses are relatively low compared with helical torsion springs. Because of this, backlash and deformation on the outer ends is usually reduced [39]. Since none of the coils normally come in contact with each other, friction losses do not occur. Due to this, spiral springs provide a linear torque profile.

A spiral spring together with the nomenclature used to describe it can be seen in Fig. 8. The equations used for this type of springs are shown in Table VII.

$$\sigma_{max} = K_b \frac{6M}{bt^2} \quad (34)$$

$$\sigma_{zul} = 0.75 R_m \quad (35)$$

$$\varphi = \frac{12ML}{Ebt^3} \quad (36)$$

$$m \approx \rho \pi n b t (R_i + R_o) \quad (37)$$

$$R_m = A_m - B_m \log t \quad (38)$$

$$U = \frac{1}{2} M \varphi \quad (39)$$

$$V \approx \pi R_o^2 b \quad (40)$$

$$L = n\pi(R_i + R_o) \quad (41)$$

TABLE VII: Equations of flat spiral springs

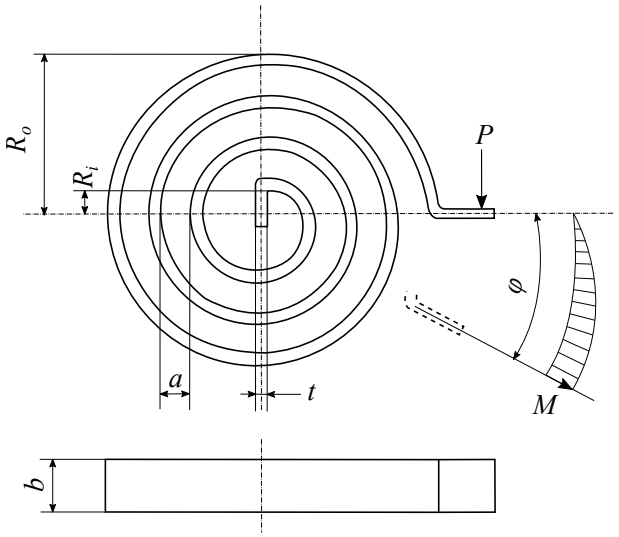

Fig. 8: Representation of spiral springs and the used nomenclature.

To start the derivations it should be noted that again the assumption is made that $n = n_t$.

To continue, the logarithm in (38) is again replaced by a power law, such that (35) becomes:

$$\sigma_{zul} = A t^B \quad (42)$$

A table of the different coefficients A and B for springs of different catalogs is given in Table VIII.

Catalog		Power law: Ad^B		R^2
		$A/1e6$	B	
Lesjöfors [37]	Lifetime = 10.000 cycles	763.1	-0.09675	0.971
	Lifetime = 100.000 cycles	611.5	-0.09648	0.970

TABLE VIII: Coefficients A and B for different spiral torsion springs proposed in catalogs.

1) ***Energy storage capacity vs. Mass***:

We start by deriving an equation which describes the load as a function of the wire diameter. The maximum tensile strength of helical torsion springs can be written as a power law. Hence, by combining Eqs. (34), (35) and (38), the following relation can be found:

$$\sigma_{max} = K_b \frac{6M}{bt^2} = A t^B \rightarrow M = \frac{A b t^{2+B}}{6K_b} \quad (43)$$

Knowing that $U = \frac{1}{2} M \varphi$, combined with Eqs. (36) and (43), it can be derived that the energy capacity inside a spiral spring is given by:

$$U = \frac{A^2 t^{2B}}{6\rho K_b^2 E} m \quad (44)$$

By implementing the influence of the spring thickness (t), using Eq. (37), Eq. (44) can be written as:

$$U = \frac{A^2}{6K_b^2 E}\rho^{-2B-1}\left(\pi n b(R_i+R_o)\right)^{-2B} m^{2B+1} \tag{45}$$

Hence, in order to maximize the energy capacity as a function of the volume, the number of coils, the strip width and the inner and outer diameter of the coil should be maximized.

With this knowledge, Eq. (45) can be used to see how the energy storage capacity evolves as a function of the mass. This behaviour is depicted in Fig. 9.

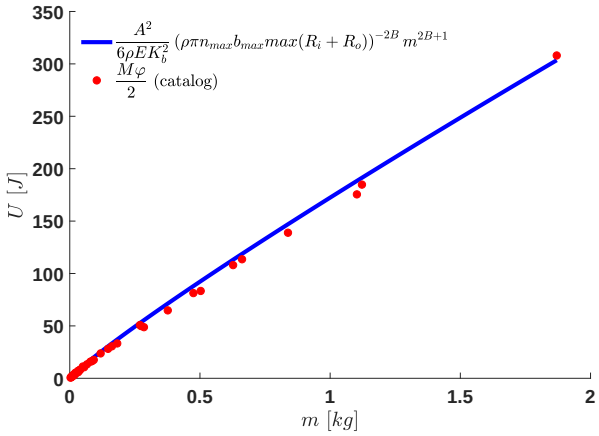

Fig. 9: The red dots represent the energy storage capacity of spiral springs as a function of their mass. This data is extracted from the Lesjöfors catalog [37]. The blue line represents the maximum energy storage capacity according to Eq. (45). The maximum number of coils, maximum spring width and maximum spring index in the catalog were taken for C, b and n.

*2) **Energy storage capacity vs. Volume**:*

To find the volumetric energy density, again the same procedure will be followed. However, the problem is now that Eq. (40) does not give a relationship between the thickness t and the volume V. Hence, to solve this, the width b will be used to insert the volume into the equation. Thus, by inserting Eqs. (36), (40) and (43) into Eq. (39), it can be found that the energy capacity inside a spiral spring as a function of its volume, is given by:

$$U = \frac{A^2 n t^{2B+1}(R_i+R_o)}{6K_b^2 E R_o^2} V \tag{46}$$

This equation maximal when both n, t and $(R_i+R_o)/R_o^2$ are maximized. It is however noted in Fig. 10 that the manufacturer from which the data was taken, only maximized the factor R_i+R_o. This is most likely due to the fact that in the industry a preference is given to maximize the energy density as a function of its mass and for that purpose indeed the factor R_i+R_o needs to be maximized. Taking this into account, it can be noted that applications where the volume is limited, catalog springs will not provide the best solutions.

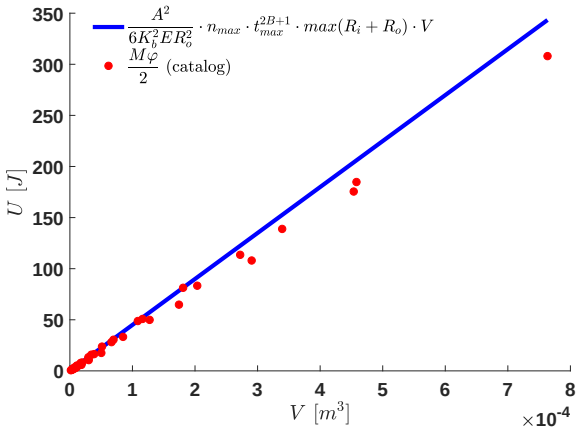

Fig. 10: The red dots represent the energy storage capacity of spiral springs as a function of their enclosed volume. This data is extracted from the Lesjöfors catalog [37]. The blue line represents the maximum energy storage capacity according to Eq. (46). The maximum number of coils and maximum spring index in the catalog were taken for C and n.

IV. INFLUENCE OF PARALLELIZATION

A. Introduction

In this section, the influence of parallelization will be investigated again based on the stress equations of each respective spring. To quantify the reduction in mass and enclosed volume with the number of parallel springs, it will be assumed in the equations that a single spring is replaced by N identical springs in parallel. In a parallel arrangement all springs have the same extension δ or angular deflection φ as the single spring they replace (dependent on how they are loaded). However, respectively the load and the torque on each spring is divided by N.

B. Compression springs

When more than one compression spring is coupled in parallel, the load on each spring is divided by the number of springs. Using this, one can find by equaling Eq. (1) and Eq. (11) that, for a given load, the coil diameter as a function of number of springs is given by:

$$\begin{aligned}\tau_{c,zul} &= A d^B \\ &= K\frac{8\frac{P}{N}Cd}{\pi d^3} \\ &= \tau_{max}\end{aligned} \tag{47}$$

From which it follows that:

$$d = \left(\frac{8KPC}{A\pi}\right)^{\frac{1}{B+2}} N^{\frac{-1}{B+2}} \tag{48}$$

By setting the desired extension, it is possible to find the number of active coils required.

$$\begin{aligned}\delta &= \frac{8\frac{P}{N}C^3 n}{Gd} \\ n &= \frac{\delta GdN}{8PC^3} \\ &= \frac{\delta G}{8PC^3}\left(\frac{8KPC}{A\pi}\right)^{\frac{1}{B+2}} N^{\frac{B+1}{B+2}}\end{aligned} \tag{49}$$

The mass can thus be computed multiplying Eq. (4) with N. After some small calculations, we find that:

$$m \approx \frac{\rho\pi^2\delta G}{32PC^2}\left(\frac{8KPC}{A\pi}\right)^{\frac{4}{B+2}} N^{\frac{B-2}{B+2}} \tag{50}$$

The reduction of mass given by the parallel arrangement is denoted by $O(m)$ and is given by:

$$O(m) = \frac{m(N)}{m(N=1)} = N^{\frac{B-2}{B+2}} \tag{51}$$

Another question regarding the parallel configuration is the space required in comparison with a single spring (and this in term of the height and diameter). The height $h_{parallel}$ and the volume $V_{parallel}$ can be approximated by:

$$\begin{cases} h_{parallel} \propto nd \\ V_{parallel} \approx N h_{parallel}\pi(D+d)^2/4 \end{cases} \tag{52}$$

By using this, also $O(h)$ and $O(V)$ can be computed:

$$O(h) = N^{\frac{B}{B+2}} \tag{53}$$

$$O(V) = N^{\frac{2B}{B+2}} \tag{54}$$

It is hard to make a fair comparison between the 2 configurations, because there are several ways to replace a single spring by multiple, which often depend on the available space. A possible way to replace one spring by multiple is for example 'circle packing'. This is a method where circles of small diameters (parallel arrangement) are placed inside a circle of bigger diameter (single spring being replaced) is possible. Another method, already used for long time, consists of placing compression springs inside of each other. This method is called "*spring nesting*". Nonetheless, the conclusion is that a parallel arrangement of springs can be used to increase the energy storage capacity, both as a function of mass and volume.

C. Torsion springs

When more than one torsion spring is coupled in parallel, the torque on each spring is divided by the number of springs. Using this, one can find by equaling Eq. (21) and Eq. (29) that for a given torque, the coil diameter as a function of number of springs is given by:

$$\begin{aligned}\sigma_{zul} &= Ad^B \\ &= K\frac{32\frac{M}{N}}{\pi d^3} \\ &= \sigma_{max}\end{aligned} \tag{55}$$

From which it follows that:

$$d = \left(\frac{32M}{A\pi}\right)^{\frac{1}{B+3}} N^{\frac{-1}{B+3}} \tag{56}$$

By setting the desired angular deflection, it is possible to find the number of active coils required.

$$\begin{aligned}\varphi &= \frac{64\frac{M}{N}Cn}{Ed^3} \\ n &= \frac{\varphi Ed^3 N}{64MC} \\ &= \frac{\varphi E}{64MC}\left(\frac{32M}{A\pi}\right)^{\frac{3}{B+3}} N^{\frac{B}{B+3}}\end{aligned} \tag{57}$$

The mass can thus be computed multiplying Eq. (24) with N. After some small calculations, we find that:

$$m \approx \frac{\rho\pi^2\varphi E}{256M}\left(\frac{32M}{A\pi}\right)^{\frac{6}{B+3}} N^{\frac{2B}{B+3}} \tag{58}$$

The reduction of mass given by the parallel arrangement is denoted by $O(m)$ and is given by:

$$O(m) = \frac{m(N)}{m(N=1)} = N^{\frac{2B}{B+3}} \tag{59}$$

Now we can again calculate the influence on the height and volume:

$$\begin{cases} h_{parallel} \approx nd \\ V_{parallel} \approx N h_{parallel}\pi(D+d)^2/4 \end{cases} \tag{60}$$

By using the previous derivations, one finds that:

$$O(h) = N^{\frac{B-1}{B+3}} \tag{61}$$

$$O(V) = N^{\frac{2B}{B+3}} \tag{62}$$

The fact that B has a small negative value, i.e. $-1 < B < 0$ (see Table V), indicates that applying multiple parallel springs is very beneficial in terms of size reduction. Especially height is affected positively.

D. Spiral torsion springs

When more than one torsion spring is coupled in parallel, the torque on each spring is divided by the number of springs. Using this, one can find by equaling Eq. (34) and Eq. (42) that for a given torque, the coil diameter as a function of number of springs is given by:

$$\begin{aligned}\sigma_{zul} &= At^B \\ &= K_b \frac{6\frac{M}{N}}{bt^2} \\ &= \sigma_{max}\end{aligned} \tag{63}$$

From which it follows that (if we consider $K_b = 1$):

$$t = \left(\frac{6M}{Ab}\right)^{\frac{1}{B+2}} N^{\frac{-1}{B+2}} \tag{64}$$

This is however not the only thing that needs to be used to do a good analysis. Eq. (64) implies actually that when one big spring is replaced, the width (b) is kept fixed to the original one, i.e. only t, R_i and R_o can change when applying parallelization. To avoid this, it can be noted that there is actually a connection between the thickness (t) and width of the spring (b). It is recommended that the ratio $\frac{b}{t}$ used by manufacturers is limited. In this paper this ratio will be denoted by Q. This is reflected in standards, e.g. $Q = \frac{b}{t} \in [1;15]$ for DIN 2090 and DIN 10132-4. It can be seen that this recommendation is followed, since the spiral springs made by Lesjöfors are also bounded ($Q \in [5.5;10]$).

By implementing this, Eq. (64) becomes:

$$t = \left(\frac{6M}{AQ}\right)^{\frac{1}{B+3}} N^{\frac{-1}{B+3}} \tag{65}$$

By setting the desired angular deflection, it is possible to find the number of active coils required.

$$\begin{aligned}\varphi &= \left(\frac{12\frac{M}{N} n\pi (R_i + R_o)}{Ebt^3}\right) \\ n &= \frac{\varphi E Q t^4 N}{12\pi M (R_i + R_o)} \\ &= \frac{\varphi E Q}{12\pi M (R_i + R_o)} \left(\frac{6M}{AQ}\right)^{\frac{4}{B+3}} N^{\frac{B-1}{B+3}}\end{aligned} \tag{66}$$

The mass can thus be computed by multiplying Eq. (37) with N, i.e. :

$$m \approx N\rho\pi nbt(R_i + R_o) \tag{67}$$

Here it can be seen that the influence of the inner and outer radius also plays a role and that this is also a factor that can change when parallelization is applied.

First, a look can be given to R_o, since this will also play a role in the volume scaling. R_o can be approximated by assuming first the case where there is no spacing between all the coils. In this case, it can easily be seen that $R_o \propto nt$. However, in order to not have friction, spiral springs do have a fixed spacing between each of the coils. To implement this behaviour, which will be different for each manufacturer, a coefficient γ will be used to adjust to the correct design, i.e. :

$$R_o = \alpha (nt)^\gamma \tag{68}$$

Since $R_i = R_o - n(t + a)$ (a can be written as a multiple of the thickness (t)), the same power law can be applied for both R_o and $(R_i + R_o)$. This will only result in a small change of the coefficients α and γ, since R_i is rather small, as can be seen in Table IX.

Catalog		Power law: $\alpha (n \cdot t)^\gamma$		R^2
		α	γ	
Lesjöfors [37]	R_o	1.84	0.839	0.991
	$R_i + R_o$	1.98	0.765	0.995

TABLE IX: Coefficients α and γ for different spiral torsion springs proposed in catalogs.

Implementing this in Eq. (67) gives that the reduction of mass given by the parallel arrangement is given by:

$$O(m) = \frac{m(N)}{m(N=1)} = N^{\frac{2B}{B+3}} \tag{69}$$

Now we can again calculate the influence of the volume:

$$V_{parallel} \approx N\pi R_o^2 b \tag{70}$$

After some straightforward calculations (assuming that α_1 and γ_1 are used to represent the power law of R_o and α_2 and γ_2 to represent the power law of $R_i + R_o$, in order to make a proper distinction between them), it can be found that the reduction of the enclosed volume is given by:

$$O(V) = N^{\frac{2\gamma_1(B-2)+(B+2)(1+\gamma_2)}{(B+3)(1+\gamma_2)}} \tag{71}$$

E. Overview

Since now the influence of parallelization for every spring is derived, they can be plotted against each other based on catalog data.

Fig. 11 visualizes the gain in (a) mass and (b) enclosed volume when one spring is replaced by N smaller ones. Here, it can clearly be seen that compression springs are superior for both metrics. In terms of parallelization, spiral springs are seen to be the worst, since they tend to have a comparable mass and enclosed volume when a big unit is replaced by several smaller ones.

V. PRACTICAL CASE STUDY

A. Introduction

Compression springs are the most common type of springs used in actuator design and they are also the ones that show the most promising results for parallelization. A case study will therefore be done to demonstrate the effects of parallelization for the practical design of a compression spring.

Initially, a theoretical derivation will be given to see how each of the mechanical sub-components, necessary for the complete construction, will scale with the parallelization. Afterwards, this theoretical derivation will be tested by selecting one specific spring from the Alcomex catalog and replacing it by multiple smaller ones that overall provide the same characteristics.

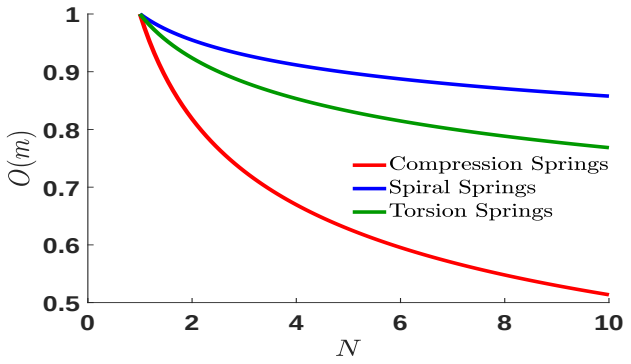

(a) Effect of parallelization in terms of mass for compression-, spiral- and torsion springs.

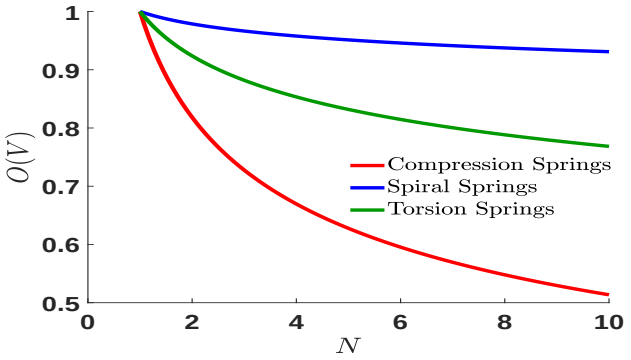

(b) Effect of parallelization in terms of enclosed volume for compression-, spiral- and torsion springs.

Fig. 11: Representation of the gain in (*a*) mass and (*b*) enclosed volume when one spring is replaced by N smaller ones. The effect of parallelization is shown for all discussed types of springs, i.e. compression-, spiral- and torsion springs and the found behaviour is based on catalog data. From these graphs it can clearly be seen that compression springs are superior and that spiral springs have the smallest benefit in terms of parallelization.

B. Theoretical derivation

In a practical case there are different possible arrangements, depending on the application. In this case study we will use the particular design depicted in Fig. 12.

Fig. 12 contains four variables, which are given by:

$$\begin{cases} D_1 & = (D+d)\left(1+\frac{1}{sin(\frac{\pi}{N})}\right) \\ H_1 & = constant \\ D_2 & = D-d \\ H_2 & = \frac{L_0}{5} \end{cases} \tag{72}$$

In this design, springs are placed to minimize the required space/volume. The topology used in these derivations is depicted in Fig. 13. This topology does not take some clearance into account between the springs (which is normally necessary, since springs expand laterally when compressed) in order to simplify the derivations. According to these design rules, the diameter of the supporting disc, D_1, can be calculated by the formula displayed in Eq. (72). This formula is however only valid starting from $N = 2$, but this is no problem, since $N = 1$ is the reference.

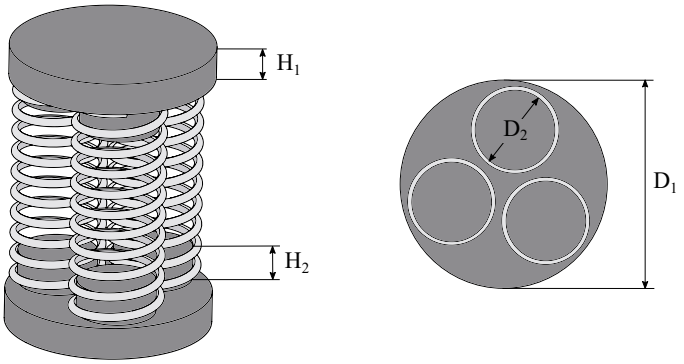

Fig. 12: Representation of the compression spring arrangement with all the size parameters.

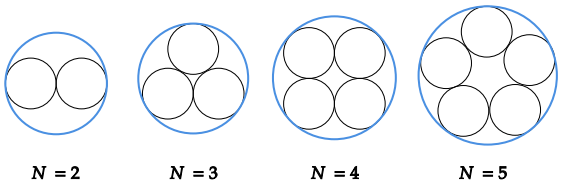

Fig. 13: Representation of the topology of the compression springs (black) and the holding disc (blue) as a function of the used parallelization number.

The thickness H_1 of the supporting discs is typically constant for a given applied load. Hence, if the parallelization is applied, the total load on the disc will remain the same. Due to this, there is no effect on the thickness of the supporting discs, when one big spring is replaced by multiple smaller ones.

Each of the springs also needs a small pin on both ends that guides the coil to avoid buckling and sliding away. This pin can have a theoretical maximum diameter of $D_2 = D - d$. In practice there must be a clearance of a few *mm*, but since this will not affect the scaling (since this clearance stays approximately constant), the theoretical value will not be changed. Note that since these pins only have a guiding function, they can be made hollow. For simplicity and due to the fact that this will not affect the scaling, this will however not be done.

The height of the pins, H_2, is proportional to the free length of the spring L_0, since the pins are necessary to avoid buckling. Hence, the higher the free length, the higher the height of the pins. In this case it is chosen to take approximately $1/5$th of the total free length.

C. Energy storage capacity vs Mass

When looking to the different components, displayed in Fig. 12, the total mass can be written as:

$$m_{total} = m_{springs} + m_{discs} + m_{pins} \tag{73}$$

By filling in everything, this can be approximated by:

$$m_{total} \approx N \frac{\rho\pi^2\delta G}{32PC^2}\left(\frac{8KPC}{A\pi}\right)^{\frac{4}{B+2}} N^{\frac{B-2}{B+2}} + 2\rho\frac{D_1^2\pi}{4}H_1 + 2N\rho\frac{D_2^2\pi}{4}H_2 \tag{74}$$

From this equation, it can be noted that the three separate terms cannot be combined. A way to still see the influence of parallelization on a practical set-up, the scaling laws of each separate part should be derived:

$$\begin{cases} m_{springs} & \approx \frac{\rho\pi^2\delta G}{32PC^2}\left(\frac{8KPC}{A\pi}\right)^{\frac{4}{B+2}} N^{\frac{2B}{B+2}} \\ m_{discs} & = \frac{\rho\pi}{2}\left[(D+d)\left(1+\frac{1}{sin(\frac{\pi}{N})}\right)\right]^2 H_1 \\ m_{pins} & = \frac{N\rho\pi}{10}(D-d)^2 L_0 \end{cases} \tag{75}$$

By filling in Eqs. (48) and (49) together with the assumption that H_1 is constant and $L_0 \propto nd$, it can be written that the masses scale like:

$$\begin{cases} O(m)_{springs} & = N^{\frac{2B}{B+2}} \\ O(m)_{discs} & = N^{\frac{-2}{B+2}}\left(1+\frac{1}{sin(\frac{\pi}{N})}\right)^2 \\ O(m)_{pins} & = N^{\frac{2B}{B+2}} \end{cases} \tag{76}$$

The curve that shows the scaling law of each of these parts, is depicted in Fig. 14. This graph shows that parallelization is beneficial for each of the components, except for the holding discs.

D. Energy storage capacity vs Volume

The total enclosed volume is given by:

$$V_{total} = (h_{spring} + 2H_1)\frac{D_1^2\pi}{4} \tag{77}$$

Hence, this has to be written again into several parts, namely the contribution of the springs and the contribution of the holding discs. Since H_1 is constant, both volumes are proportional to:

$$\begin{cases} V_{springs} & \propto nd\left[(D+d)\left(1+\frac{1}{sin(\frac{\pi}{N})}\right)\right]^2 \\ V_{discs} & = \left[(D+d)\left(1+\frac{1}{sin(\frac{\pi}{N})}\right)\right]^2 \end{cases} \tag{78}$$

Filling in Eqs. (48) and (49), makes that the practical volume scales like:

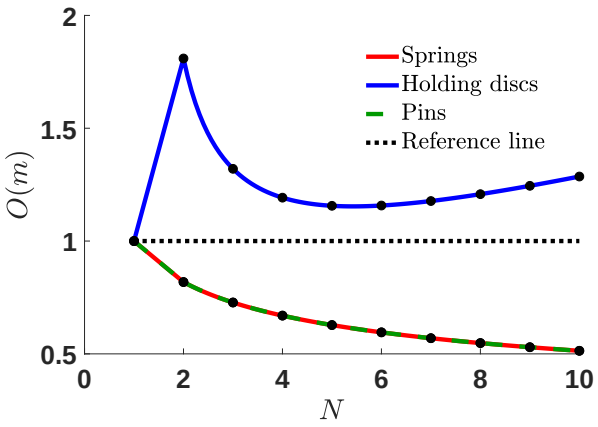

Fig. 14: Representation of the gain in mass of a practical compression spring arrangement when one spring is replaced by N smaller ones. Here, the red line represents the scaling of the spring mass, the blue line represents the scaling of the holding discs mass and the green line represents the scaling of the mass of the guiding pins. The dotted black line represents the reference mass for each of the components when only 1 spring is used. In this graph, it is visualized that in the complete arrangement of a compression spring, both the springs and guiding pins always benefit from the parallelization. The holding discs will however never have benefit from this.

$$\begin{cases} O(V)_{springs} & = N^{\frac{B-2}{B+2}}\left(1+\frac{1}{sin(\frac{\pi}{N})}\right)^2 \\ O(V)_{discs} & = N^{\frac{-2}{B+2}}\left(1+\frac{1}{sin(\frac{\pi}{N})}\right)^2 \end{cases} \tag{79}$$

The curve that shows this scaling law is depicted in Fig. 15. This graph shows that the used topology technique of the springs (see Fig. 13) is no longer optimal after $N = 6$.

The conclusion can also be made that the gain for energy storage capacity as a function of the volume is rather limited.

E. Practical application

Now, for the practical application, a compression spring is chosen from the Alcomex catalog. The characteristics of this spring are shown in Table X.

d	=	5	mm	F_{max}	=	1021.12	N
D	=	32	mm	k	=	19.03	$\frac{N}{mm}$
C	=	6.40	/	D_2	=	26	mm
n	=	8.5	/	L_0	=	110	mm
m	=	130.87	g	L_n	=	57.5	mm

TABLE X: Characteristics of the selected big spring (Alcomex compression spring, part number DR3850 [36]).

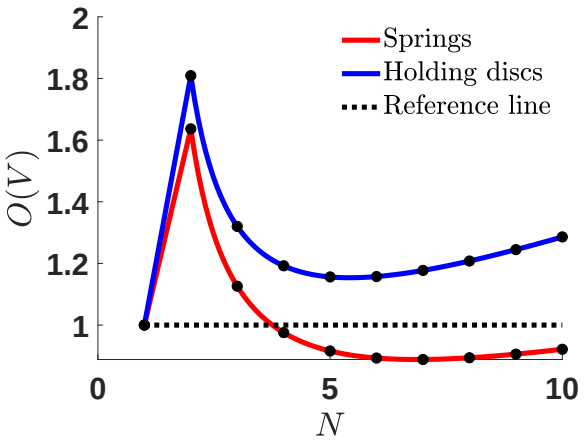

Fig. 15: Representation of the gain in enclosed volume of a practical compression spring arrangement when one spring is replaced by N smaller ones. Here, the red line represents the scaling of the enclosed volume of the spring and the blue line represents the scaling of the holding discs. The dotted black line represents the enclosed volume of a spring arrangement that uses only 1 spring.

Looking to the theoretical derivations in the previous subsection, it is chosen to replace the chosen spring by 5 smaller ones, i.e. $N = 5$, since this is a value for which already some differences should be seen.

These smaller springs should have the same behaviour and hence should provide the same deflection, a spring constant which is approximately $1/5$th of the big one, a maximum force which is approximately $1/5$th of the original one and a similar spring index. In order to find the correct smaller springs, some of the theoretical scaling laws can be used, namely Eqs. (48) and (49).

$$\begin{cases} d_{small} & = d_{big} N^{\frac{-1}{B+2}} = 5mm \cdot 5^{\frac{-1}{1.7472}} = 1.99mm \\ D_{small} & = C_{big} d_{small} = 6.40 \cdot 1.99mm = 12.74mm \\ F_{max,small} & = \frac{F_{max,big}}{N} = \frac{1021.12N}{5} = 204.2240N \\ k_{small} & = \frac{k_{big}}{N} = \frac{19.03 \frac{N}{mm}}{5} = 3.806 \frac{N}{mm} \\ n_{small} & = n_{big} N^{\frac{B+1}{B+2}} = 8.5 \cdot 5^{\frac{0.7472}{1.7472}} = 16.92 \end{cases} \tag{80}$$

According to these calculations, a spring was found with similar characteristics. The characteristics of this spring are shown in Table XI.

d	=	2	mm	F_{max}	=	211.57	N
D	=	12.5	mm	k	=	3.77	$\frac{N}{mm}$
C	=	6.25	/	D_2	=	9.9	mm
n	=	18.5	/	L_0	=	105	mm
m	=	17.80	g	L_n	=	47.2	mm

TABLE XI: Characteristics of the selected small springs (Alcomex compression spring, part number DR2690 [36]).

Since now the replacement springs are found, the size and mass of the springs and their sub-components can be calculated.

1) Compression springs:

When comparing the big spring with the 5 small springs in terms of mass, it can immediately be calculated that there is indeed a mass decrease when parallelization is applied:

$$O(m)_{springs} = \frac{5 \cdot 17.80g}{130.87g} = 0.68 \tag{81}$$

This is close to the theoretical law, which predicted that $O(m)_{springs} = 0.63$ (see Fig. 14).

To see the contribution of the spring arrangement on the enclosed volume, the volume needs to be calculated for both $N = 1$ and $N = 5$. For the one big spring, the enclosed volume is given by:

$$V_{spring,big} = \frac{\pi \left(D_{big} + d_{big}\right)^2}{4} L_{0,big} = 1.1827 \cdot 10^{-4} m^3 \tag{82}$$

Using Eq. 72, the enclosed volume of the 5 small springs can be calculated:

$$\begin{aligned} V_{springs,small} &= \frac{\pi \left[\left(D_{small} + d_{small}\right)\left(1 + \frac{1}{sin(\frac{\pi}{N})}\right)\right]^2}{4} L_{0,small} \\ &= 1.2652 \cdot 10^{-4} m^3 \end{aligned} \tag{83}$$

Now the parallelization effect of the springs on the enclosed volume can be calculated:

$$O(V)_{springs} = \frac{1.2652 \cdot 10^{-4} m^3}{1.1827 \cdot 10^{-4} m^3} = 1.07 \tag{84}$$

This value is larger than the predicted 0.92, which can be seen in Fig. 15. This is most likely due to the high L_0 of the small springs. Normally, replacement springs should be chosen with the following characteristic:

$$\left(\frac{L_0}{nd}\right)_{big} \approx \left(\frac{L_0}{nd}\right)_{small} \tag{85}$$

However, there was no spring available in the catalog that had all the previous requirements and also a correct L_0. If a correct spring could have been found for which Eq. (85) is valid, its L_0 would have to be around $95mm$. Filling in this length in the volume calculations would have resulted in an enclosed volume of the springs, which is $1.1447 \cdot 10^{-4} m^3$, Calculating the parallelization effect of this volume would result in $O(V)_{springs} = 0.96$, which is a lot closer to the theoretical value.

2) Holding discs:

In order to calculate the mass and enclosed volume of the discs, its size parameters need to be determined. The diameter of the discs is completely determined by the number and size of the springs:

$$\begin{cases} D_{1,big} & = \left(D_{big} + d_{big}\right) \\ & = 37.00mm \\ D_{1,small} & = \left(D_{small} + d_{small}\right)\left(1 + \frac{1}{sin(\frac{\pi}{N})}\right) \\ & = 39.17mm \end{cases} \tag{86}$$

The thickness on the other hand, is completely determined by the load. In this case study it is assumed that the load will go to the maximum allowable force of the springs. After applying some stress simulations it was found out that a thickness of $H_1 = 5mm$ was enough when an aluminum plate ($\rho = 2700\frac{kg}{m^3}$) was used as holding disc.

Hence, the mass of the holding discs for the one big spring and for the multiple small springs, is given by:

$$\begin{cases} m_{discs,big} & = 2\left(\frac{\rho\pi D_{1,big}^2}{4}\right)H_1 \\ & = 29.03g \\ m_{discs,small} & = 2\left(\frac{\rho\pi D_{1,small}^2}{4}\right)H_1 \\ & = 32.53g \end{cases} \tag{87}$$

When comparing both cases, it can immediately be calculated that there is indeed a mass increase when parallelization is applied:

$$O(m)_{discs} = \frac{32.53g}{29.03g} = 1.12 \tag{88}$$

This is close to the theoretical law, which predicted that $O(m)_{discs} = 1.16$ (see Fig. 14).

To find the enclosed volume of the discs, again both cases need to be calculated. For this it can intuitively be seen that $O(v)_{discs} = O(m)_{discs}$, since they use the same scaling law.

However, the volume still needs to be calculated exactly for both the cases, since the relative contribution of each part will need to be calculated at the end. The volume of each of the cases is:

$$\begin{cases} V_{discs,big} & = 2\left(\frac{\pi D_{1,big}^2}{4}\right)H_1 \\ & = 1.0752 \cdot 10^{-5}m^3 \\ V_{discs,small} & = 2\left(\frac{\pi D_{1,small}^2}{4}\right)H_1 \\ & = 1.2050 \cdot 10^{-5}m^3 \end{cases} \tag{89}$$

3) Guiding pins:

The last part remaining are the guiding pins. They do not contribute to the enclosed volume calculations, since they are internal parts. Hence, only there mass needs to be calculated. Considering that H_2, the height of the pins, is given by $L_0/5$ and that D_2 is given in the datasheet (see Tables X and XI), the total mass of all pins can be calculated for both cases:

$$\begin{cases} m_{pins,big} & = \frac{\rho\pi}{10}D_{2,big}^2 L_0 \\ & = 63.07g \\ m_{pins,small} & = \frac{N\rho\pi}{10}D_{2,small}^2 L_0 \\ & = 43.64g \end{cases} \tag{90}$$

When comparing both cases, it can immediately be calculated that there is indeed a mass decrease when parallelization is applied:

$$O(m)_{pins} = \frac{43.64g}{63.07g} = 0.69 \tag{91}$$

This is close to the theoretical law, which predicted that $O(m)_{pins} = 0.63$ (see Fig. 14).

4) Complete arrangement:

In order to see the influence of parallelization on the total arrangement, all separate terms need to be added:

$$\begin{aligned} O(m)_{total} &= \frac{m_{springs,small} + m_{discs,small} + m_{pins,small}}{m_{spring,big} + m_{discs,big} + m_{pins,big}} \\ &= \frac{89g + 32.53g + 43.64g}{130.87g + 29.03g + 63.07g} \\ &= 0.74 \end{aligned} \tag{92}$$

This means that parallelization is indeed useful for mass reduction. It can also be calculated if the same can be said about volume scaling.

$$\begin{aligned} O(V)_{total} &= \frac{V_{springs,small} + V_{discs,small}}{V_{spring,big} + V_{discs,big}} \\ &= \frac{1.2652 \cdot 10^{-4}m^3 + 1.2050 \cdot 10^{-5}m^3}{1.1827 \cdot 10^{-4}m^3 + 1.0752 \cdot 10^{-5}m^3} \\ &= 1.07 \end{aligned} \tag{93}$$

This result indicates that there would be an increase in volume when parallelization is applied. However, when $O(V)_{total}$ would be calculated with the adapted springs (the one with $L_0 = 95mm$), $O(V)_{total}$ would become 0.98.

It can be concluded that, as the theoretical development predicted, parallelization is indeed useful for mass reduction. It has however a very limited effect on the volume. Better topologies (e.g. spring nesting) and/or more parallel springs could potentially provide better solutions.

VI. DISCUSSION

A. Non-treated Springs

In this work, we have covered scaling laws for compression, torsion and spiral springs. There are, however, a wide range of different spring designs, which are not treated in this work for a variety of reasons. A few examples are given below.

1) Tension Springs:

Tension springs, just like compression springs, are helical springs and rely on the same design principles. Basically the only difference is that the forces on them are applied in different directions. This, in turn, leads to two different mechanical properties:

- The end coils: Tension springs generally end with a hook. The stresses in this hook can be high due to its curvature. This limits the load that can be applied to the spring. Consequently, unlike compression springs, the coils of extension springs are not loaded to their limit.
- The initial tension: Before tension springs start to deform, an initial tension must be applied to the springs. This manifests itself as a dead zone in the force-extension characteristic. Compression springs do not exhibit this behaviour.

This implies that the derivation of the scaling laws for tension springs should be done with the stress equations of the hooks, since these will be the places where failure will occur if used correctly. Consequently, a lot of information is needed about the shape of these hooks to calculate these stresses. This is however commonly not known in catalogs. Combined with the fact that a lot of hook shapes exist, it becomes impossible to validate a theoretical law, since not all needed data can be retrieved.

2) Leaf Springs:

Leaf springs are flat sections of springs that are either clamped on one end and loaded on the other or clamped at both extremities and loaded in the middle. These leaf springs can be stacked in one or multiple layers.

With so many possible arrangements and shapes of the strip of metal itself, this type of springs is usually custom-made.

As a result, no catalog data can be found to verify a theoretical law. Hence, verification of any developed scaling law would be tedious, which is why we decided not to tackle them for this type of spring.

3) Constant Force Springs:

A constant force spring is a pre-stressed flat strip of spring material which is formed into an almost constant radius that can be coiled around itself (with a inner bearing) or around a drum. When the spring is extended, i.e. deflected, the extended material straightens. This straightening causes internal stresses, since the spring tries to resist the applied load in order to restore its natural radius. This behaviour can be compared to a normal extension spring, but with a nearly constant (zero) rate, so constant force, since the natural radius is almost constant.

The rated force of the spring is reached after the deflection has reached a length equal to 1.25 times its diameter. After this, the force stays relatively constant regardless of the extension length. The rated force is determined by the thickness and width of the material and the diameter of the coil.

The problem for applying scaling laws on constant force springs is the fact that each manufacturer takes different safety factors into account for each spring, even within the same catalog. As a result, no clear scaling can be found between the thickness of the springs and the maximum stress inside, whereas for other types of springs this scaling is normally found with at least 90% accuracy.

For this reason a theoretical law can be derived, but no *A* and *B* factor can be determined for the constant force springs. Since this is the basis of the entire analysis, this can not be verified with catalog data, which is the reason why it is not included in this paper.

B. Comparison of different types of springs

To compare the maximum achievable energy storage capacity of different springs as a function of their mass and their enclosed volume, a plot is depicted in Fig. 16.

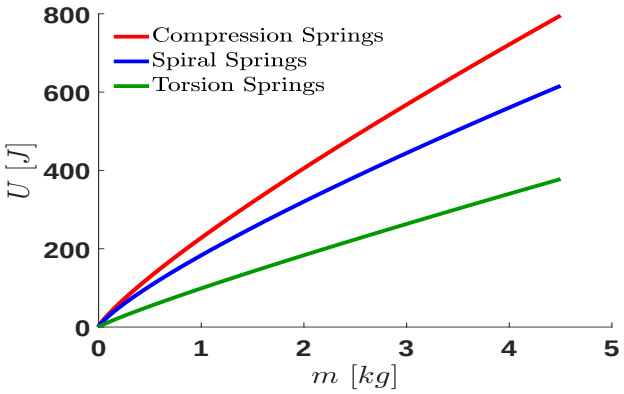

(a) Energy storage capacity as a function of the mass.

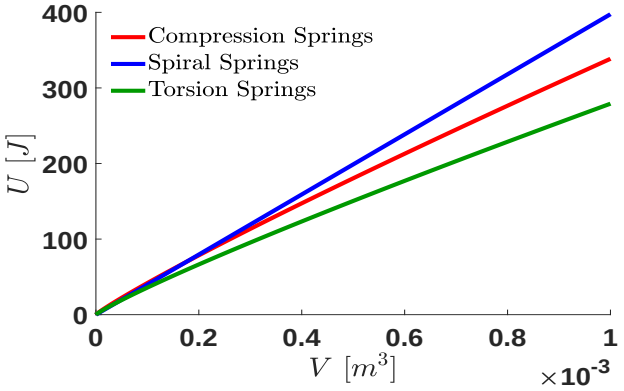

(b) Energy storage capacity as a function of the volume.

Fig. 16: Representation of the maximum achievable energy storage capacity as a function of (a) their mass and (b) their enclosed volume. These lines are plotted for all discussed types of springs, i.e. compression-, spiral- and torsion springs. These optimal lines are based on catalog data. From these graphs it can be seen that compression springs are superior when mass is the metric, but that spiral springs are slightly better for energy storage capacity as a function of the enclosed volume. This difference would however increase for bigger volumes, since spiral springs follow a linear law.

Here, it can be seen that compression springs perform better for energy storage capacity as a function of its mass. Regarding the energy capacity as a function of the enclosed volume, they are however not anymore the best, except for the region of small volumes where they are approximately equal to torsion springs and slightly better than spiral springs. For bigger volumes spiral springs are the best, which is due to their linear correlation with the enclosed volume. Torsion springs can be considered to be the worst for both metrics.

Taking this into account, in addition to the conclusions made for parallelization, it can be said that in terms of energy storage capacity both for the use of one big spring or several smaller ones in parallel, compression springs are usually the best choice, however, the application matters too.

C. Design guidelines

In order to design and/or select a spring for an application, when a maximized energy storage capacity is wanted (either as a function of its mass or as a function of its enclosed volume), some spring parameters need to be optimized. In Table XII an overview can be found of whether a certain parameter needs to be minimized or maximized in order to achieve maximal energy storage capacity. This overview is given for each of the discussed springs.

From this table it can be concluded that for each application, a maximal number of coils is advisable.

Energy storage capacity	vs. Mass		vs. Volume	
	Maximize	Minimize	Maximize	Minimize
Compression spring	C, n	/	n	C
Torsion spring	C, n	/	n	C
Spiral spring	n, R_i, R_o, b	/	n, t, $\frac{R_i+R_o}{R_o^2}$	/

TABLE XII: Overview of the parameters that need to be maximized and minimized for different types of springs in order to attain a maximal energy storage capacity, either as a function of their mass, either as a function of their enclosed volume.

VII. CONCLUSION

In this paper, scaling laws are derived for different types of springs with a special focus on their energy capacity and the influence of parallelization. The paper gives insights into the type of spring that provides the most benefits in terms of enclosed volume in rest condition and weight. By implementing the derived scaling laws on catalog data, it was shown that compression springs have the highest energy capacity as a function of its mass and spiral springs as a function of its enclosed volume. All these scaling laws can help to facilitate the design process, since it is now shown which parameters should be either maximized or minimized in the spring design/selection process, in order to obtain a maximal energy storage capacity as a function of either the mass or enclosed volume. To enhance the clarity of these findings, a table is made to summarize these design guidelines for when springs with optimized energy storage capacity need to be made or selected.

In this manuscript, it is also demonstrated that compression springs are the best in terms of parallelization, even without the influence of volume reducing methods, like e.g. spring nesting, which is not possible for other types of springs. This paper also shows that parallelization is in general better, which is an incentive to proceed with work regarding complex actuators, more specifically with a focus on compression springs.

This is especially relevant for redundant actuators with multiple motors and gearboxes, such as the +SPEA [30], developed in our group.

For this purpose also a practical case study was done in this paper to demonstrate how the parallelization effects a complete design with all its mechanical sub-components. This case study treated the effect of parallelization for a compression spring lay-out. The case study showed that when the sub-components are taken into account, parallelization proves to be very beneficial in terms of mass reduction, but that there is almost no effect for the volume.

Together with the known scaling laws for motors and the scaling laws for gearboxes (which are currently under investigation), future work will strive towards the development of scaling laws and design rules for a complete compliant actuator in order to optimize the design of these innovative actuators. The development of these scaling laws will also allow to develop a framework which will be able to compare all types of actuators among each other. This in order to assess the potential of complex actuators with respect to more conventional designs.

ACKNOWLEDGMENT

Elias Saerens, Stein Crispel and Tom Verstraten are all affiliated with the Research Foundation Flanders. Elias Saerens and Stein Crispel as SB PhD Fellows and Tom Verstraten as a Postdoctoral Fellow. This work has been partially funded by the European Research Council Starting Grant SPEAR (grant no. 337596).

REFERENCES

[1] G. A. Pratt and M. M. Williamson, "Series elastic actuators," in *Proceedings 1995 IEEE/RSJ International Conference on Intelligent Robots and Systems. Human Robot Interaction and Cooperative Robots*, vol. 1. IEEE, 1995, pp. 399–406.

[2] R. Van Ham, T. Sugar, B. Vanderborght, K. Hollander, and D. Lefeber, "Compliant actuator designs," *IEEE Robotics & Automation Magazine*, vol. 3, no. 16, pp. 81–94, 2009.

[3] G. Tonietti, R. Schiavi, and A. Bicchi, "Design and control of a variable stiffness actuator for safe and fast physical human/robot interaction," in *Proceedings of the 2005 IEEE international conference on robotics and automation*. IEEE, 2005, pp. 526–531.

[4] S. Wolf and G. Hirzinger, "A new variable stiffness design: Matching requirements of the next robot generation," in *2008 IEEE International Conference on Robotics and Automation*. IEEE, 2008, pp. 1741–1746.

[5] R. Van Ham, B. Vanderborght, M. Van Damme, B. Verrelst, and D. Lefeber, "Maccepa, the mechanically adjustable compliance and controllable equilibrium position actuator: Design and implementation in a biped robot," *Robotics and Autonomous Systems*, vol. 55, no. 10, pp. 761–768, 2007.

[6] D. W. Haldane, M. M. Plecnik, J. K. Yim, and R. S. Fearing, "Robotic vertical jumping agility via series-elastic power modulation," *Science Robotics*, vol. 1, no. 1, 2016.

[7] H. Yu, S. Huang, N. V. Thakor, G. Chen, S.-L. Toh, M. S. Cruz, Y. Ghorbel, and C. Zhu, "A novel compact compliant actuator design for rehabilitation robots," in *2013 IEEE 13th International Conference on Rehabilitation Robotics (ICORR)*. IEEE, 2013, pp. 1–6.

[8] R. Furnémont, G. Mathijssen, T. Van Der Hoeven, B. Brackx, D. Lefeber, and B. Vanderborght, "Torsion maccepa: A novel compact compliant actuator designed around the drive axis," in *2015 IEEE International Conference on Robotics and Automation (ICRA)*. IEEE, 2015, pp. 232–237.

[9] G. Carpino, D. Accoto, F. Sergi, N. L. Tagliamonte, and E. Guglielmelli, "A novel compact torsional spring for series elastic actuators for assistive wearable robots," *Journal of Mechanical Design*, vol. 134, no. 12, p. 121002, 2012.

[10] W. M. dos Santos, G. A. Caurin, and A. A. Siqueira, "Design and control of an active knee orthosis driven by a rotary series elastic actuator," *Control Engineering Practice*, vol. 58, pp. 307–318, 2017.

[11] M. C. Yildirim, P. Sendur, O. Bilgin, B. Gulek, G. G. Yapici, and B. Ugurlu, "An integrated design approach for a series elastic actuator: Stiffness formulation, fatigue analysis, thermal management," in *2017 IEEE-RAS 17th International Conference on Humanoid Robotics (Humanoids)*. IEEE, 2017, pp. 384–389.

[12] T. Morita and S. Sugano, "Design and development of a new robot joint using a mechanical impedance adjuster," in *Proceedings of 1995 IEEE International Conference on Robotics and Automation*, vol. 3. IEEE, 1995, pp. 2469–2475.

[13] J. Choi, S. Hong, W. Lee, S. Kang, and M. Kim, "A robot joint with variable stiffness using leaf springs," *IEEE Transactions on Robotics*, vol. 27, no. 2, pp. 229–238, 2011.

[14] M. K. Shepherd and E. J. Rouse, "Design of a quasi-passive ankle-foot prosthesis with biomimetic, variable stiffness," in *2017 IEEE International Conference on Robotics and Automation (ICRA)*. IEEE, 2017, pp. 6672–6678.

[15] A. G. Rodríguez, J. Chacón, A. Donoso, and A. G. Rodríguez, "Design of an adjustable-stiffness spring: Mathematical modeling and simulation, fabrication and experimental validation," *Mechanism and Machine Theory*, vol. 46, no. 12, pp. 1970–1979, 2011.

[16] Y. Zhu, J. Yang, H. Jin, X. Zang, and J. Zhao, "Design and evaluation of a parallel-series elastic actuator for lower limb exoskeletons," in *2014 IEEE International Conference on Robotics and Automation (ICRA)*. IEEE, 2014, pp. 1335–1340.

[17] F. Stuhlenmiller, J. Schuy, and P. Beckerle, "Probabilistic elastic element design for robust natural dynamics of structure-controlled variable stiffness actuators," *Journal of Mechanisms and Robotics*, vol. 10, no. 1, p. 011009, 2018.

[18] N. G. Tsagarakis, S. Morfey, H. Dallali, G. A. Medrano-Cerda, and D. G. Caldwell, "An asymmetric compliant antagonistic joint design for high performance mobility," in *2013 IEEE/RSJ International Conference on Intelligent Robots and Systems*. IEEE, 2013, pp. 5512–5517.

[19] T. Yokota, T. Taguchi, and M. Gen, "A solution method for optimal weight design problem of herical spring using genetic algorithms," *Computers & industrial engineering*, vol. 33, no. 1-2, pp. 71–76, 1997.

[20] K. Deb and M. Goyal, "A flexible optimization procedure for mechanical component design based on genetic adaptive search," *TRANSACTIONS-AMERICAN SOCIETY OF MECHANICAL ENGINEERS JOURNAL OF MECHANICAL DESIGN*, vol. 120, pp. 162–164, 1998.

[21] B. Kannan and S. N. Kramer, "An augmented lagrange multiplier based method for mixed integer discrete continuous optimization and its applications to mechanical design," *Journal of mechanical design*, vol. 116, no. 2, pp. 405–411, 1994.

[22] X. Qimin, L. Liwei, and X. Qili, "The optimal design and simulation of helical spring based on particle swarm algorithm and matlab," *WSEAS Transactions on Circuits and Systems*, no. 1, pp. 84–83, 2009.

[23] M. Taktak, K. Omheni, A. Aloui, F. Dammak, and M. Haddar, "Dynamic optimization design of a cylindrical helical spring," *Applied Acoustics*, vol. 77, pp. 178–183, 2014.

[24] R. Nasiri, M. Khoramshahi, M. Shushtari, and M. N. Ahmadabadi, "Adaptation in variable parallel compliance: Towards energy efficiency in cyclic tasks," *IEEE/ASME Transactions on Mechatronics*, vol. 22, no. 2, pp. 1059–1070, 2017.

[25] T. Verstraten, P. Beckerle, R. Furnémont, G. Mathijssen, B. Vanderborght, and D. Lefeber, "Series and parallel elastic actuation: Impact of natural dynamics on power and energy consumption," *Mechanism and Machine Theory*, vol. 102, pp. 232–246, 2016.

[26] E. Bolívar, S. Rezazadeh, and R. Gregg, "A general framework for minimizing energy consumption of series elastic actuators with regeneration," in *Proceedings of the ASME Dynamic Systems and Control Conference. ASME Dynamic Systems and Control Conference*, vol. 1. NIH Public Access, 2017.

[27] Y. Yesilevskiy, W. Xi, and C. D. Remy, "A comparison of series and parallel elasticity in a monoped hopper," in *2015 IEEE International Conference on Robotics and Automation (ICRA)*. IEEE, 2015, pp. 1036–1041.

[28] G. Mathijssen, D. Lefeber, and B. Vanderborght, "Variable recruitment of parallel elastic elements: Series–parallel elastic actuators (spea) with dephased mutilated gears," *IEEE/ASME Transactions on Mechatronics*, vol. 20, no. 2, pp. 594–602, 2015.

[29] G. Mathijssen, R. Furnémont, T. Verstraten, C. Espinoza, S. Beckers, D. Lefeber, and B. Vanderborght, "Study on electric energy consumed in intermittent series–parallel elastic actuators (ispea)," *Bioinspiration & biomimetics*, vol. 12, no. 3, p. 036008, 2017.

[30] G. Mathijssen, R. Furnémont, T. Verstraten, B. Brackx, J. Premec, R. Jiménez, D. Lefeber, and B. Vanderborght, "+ spea introduction: drastic actuator energy requirement reduction by symbiosis of parallel motors, springs and locking mechanisms," in *2016 IEEE International Conference on Robotics and Automation (ICRA)*. IEEE, 2016, pp. 676–681.

[31] G. Grioli, S. Wolf, M. Garabini, M. Catalano, E. Burdet, D. Caldwell, R. Carloni, W. Friedl, M. Grebenstein, M. Laffranchi *et al.*, "Variable stiffness actuators: The users point of view," *The International Journal of Robotics Research*, vol. 34, no. 6, pp. 727–743, 2015.

[32] S. Wolf, G. Grioli, O. Eiberger, W. Friedl, M. Grebenstein, H. Höppner, E. Burdet, D. G. Caldwell, R. Carloni, M. G. Catalano *et al.*, "Variable stiffness actuators: Review on design and components," *IEEE/ASME transactions on mechatronics*, vol. 21, no. 5, pp. 2418–2430, 2016.

[33] H.-J. Schorcht, M. Meissner, and U. Kletzin, "Metallfedern: Grundlagen, werkstoffe, berechnung, gestaltung und rechnereinsatz, 2. auflage," 2015.

[34] A. M. Wahl, *Mechanical springs*. Penton Publishing Company, 1944.

[35] *Normfedern - vom weltweit tätigen Partner - katalog*. BAUMANN FEDERN AG, 2018, [PDF file].

[36] *Veren uit voorraad*. Alcomex Springs, 2017, [PDF file].

[37] *The spring catalog #15*. Lesjöfors - Gas and stock springs, 2019, [PDF file].

[38] *Empowering Innovation. Engineering Value - catalog*. Century Spring Corp., 2015, [PDF file].

[39] B. T. Knox and J. P. Schmiedeler, "A unidirectional series-elastic actuator design using a spiral torsion spring," *Journal of Mechanical Design*, vol. 131, no. 12, p. 125001, 2009.